Published online 15 February 2022

Nucleic Acids Research, 2022, Vol. 50, No. 5 ***2667–2680***
https://doi.org/10.1093/nar/gkac075

SLX4 dampens MutSα-dependent mismatch repair

Jean-Hugues Guervilly*, Marion Blin†, Luisa Laureti†, Emilie Baudelet, Stéphane Audebert and Pierre-Henri Gaillard*

Centre de Recherche en Cancérologie de Marseille, CRCM, Inserm, CNRS, Aix-Marseille Université, Institut Paoli-Calmettes, Marseille, France

Received October 18, 2021; Revised January 20, 2022; Editorial Decision January 22, 2022; Accepted January 25, 2022

ABSTRACT

The tumour suppressor SLX4 plays multiple roles in the maintenance of genome stability, acting as a scaffold for structure-specific endonucleases and other DNA repair proteins. It directly interacts with the mismatch repair (MMR) protein MSH2 but the significance of this interaction remained unknown until recent findings showing that MutSβ (MSH2-MSH3) stimulates *in vitro* the SLX4-dependent Holliday junction resolvase activity. Here, we characterize the mode of interaction between SLX4 and MSH2, which relies on an MSH2-interacting peptide (SHIP box) that drives interaction of SLX4 with both MutSβ and MutSα (MSH2-MSH6). While we show that this MSH2 binding domain is dispensable for the well-established role of SLX4 in interstrand crosslink repair, we find that it mediates inhibition of MutSα-dependent MMR by SLX4, unravelling an unanticipated function of SLX4.

INTRODUCTION

Genetic integrity is constantly threatened by DNA lesions arising from both endogenous and exogenous origins. Cells rely on elaborate DNA repair and signalling pathways to fix or tolerate DNA damage, which determine cell survival and the level of mutagenesis. The human SLX4 protein contributes to many aspects of genome maintenance through multiple protein–protein interactions. One of its primary and best understood functions is how it acts as a nuclease scaffold that controls the XPF-ERCC1, MUS81-EME1 and SLX1 structure-specific endonucleases (SSE), directly modulating their catalytic activity and promoting their targeting to appropriate substrates (1–5). It makes key contributions to the repair of interstrand crosslinks (ICL) by recruiting XPF-ERCC1 to replication forks stalled by an ICL and stimulating the so-called unhooking of the lesion by XPF-ERCC1 (6,7). Recruitment of SLX4 at the ICL-stalled fork is mediated by its ubiquitin binding UBZ4 domains (8–10) and while monoubiquitinated FANCD2 has been proposed to be the UBZ4 ligand that drives SLX4 recruitment, this has been under debate (7,9–11). Moreover, recent data suggest that the E3 ligase RNF168 contributes to SLX4 targeting at ICL lesions independently of FANCD2 (12). Nevertheless, SLX4 is part of the Fanconi pathway as underscored by the identification of rare cases of bi-allelic mutations of the *SLX4/FANCP* gene causative of Fanconi Anemia (FA) (8,13). FA is a severe hereditary syndrome that is invariably characterized by a profound ICL hypersensitivity at the cellular level and is associated with bone marrow failure, developmental defects and cancer predisposition. In addition to promoting the endonucleolytic processing of ICLs by XPF-ERCC1, SLX4 is required for Holliday junction (HJ) resolution by MUS81-EME1 and SLX1 during the late steps of homologous recombination (HR) (14–16). SLX4 contributes to the maintenance of specific genomic loci such as telomeres and common fragile sites. Telomeric functions rely primarily on direct interaction with TRF2, which drives recruitment of SLX4 and its associated SSEs to chromosomes ends (17,18) as well as that of SLX4IP, which was recently shown to fulfil several important functions in telomere maintenance via the alternative lengthening of telomeres pathway (19–21). SLX4 contains SUMO-interacting motifs (SIM) that also contribute to its telomeric localization and to laser-induced DNA damage (22–24) as well as to functions of SLX4 in the maintenance of common fragile sites (CFS) (22,23) where it triggers mitotic DNA synthesis (MiDAS). Recently, SLX4 was also found to prevent replication-transcription conflicts through direct interaction with the RTEL1 helicase (25).

Hence, SLX4 exerts multiple functions in genome maintenance, each mediated by one or several protein–protein interactions. Intriguingly, the mismatch repair (MMR) factor MSH2 was also identified as a binding partner of human SLX4 (3) but the functional relevance of this interaction remained unexplored until recently (26). The primary

*To whom correspondence should be addressed. Tel: +33 486 97 73 71; Fax: +33 486 97 74 99; Email: pierre-henri.gaillard@inserm.fr
Correspondence may also be addressed to Jean-Hugues Guervilly. Email: jean-hugues.guervilly@inserm.fr
†The authors wish it to be known that, in their opinion, the second and third authors should be regarded as Joint Second Authors.
Present address: Marion Blin, Département d'Hépato-gastro-entérologie et oncologie digestive, pôle MAD, Assistance Publique des Hôpitaux de Marseille, Centre Hospitalier Universitaire de Marseille, Marseille, France.

role of MMR is to correct replication errors introduced by DNA polymerases. As such, MMR deficiency is the main cause of hereditary nonpolyposis colorectal cancer (HNPCC or Lynch syndrome) (27). MSH2 acts in the early steps of MMR and is an obligate component of the heterodimeric MutSα (MSH2-MSH6) and MutSβ (MSH2-MSH3) ATPase complexes. MutSα, which is the more abundant complex, recognizes single nucleotide mismatches and small insertion/deletions (1 or 2 nt indels) while MutSβ recognizes larger indels (28). Mismatch recognition allows the recruitment and activation of the MutLα (MLH1-PMS2) endonuclease and EXO1 exonuclease that will remove the mismatch and trigger subsequent DNA repair synthesis (29–31). Noteworthy, MMR activity is responsible for the cytotoxic effect of chemotherapeutic drugs such as the alkylating agent *N*-methyl-*N*'-nitro-*N*-nitrosoguanidine (MNNG) or the pro-drug 6-thioguanine (6-TG), which can both induce mispairing of a methylated guanine with a newly incorporated thymidine during replication and subsequent MMR activity (32).

Immunoprecipitation of overexpressed SLX4 coupled to mass spectrometry (IP-MS) analyses suggested that it associates with MutSβ (3), MutSα (33) or both complexes (34). Noteworthy, interaction between SLX4 and MutSβ, but not MutSα, was shown to stimulate HJ resolution by the SLX4–SLX1 and SLX1–SLX4–MUS81–EME1–XPF–ERCC1 (SMX) HJ resolvase complexes *in vitro* (26). Furthermore, co-depletion of MSH3 and SLX4 did not further exacerbate the phenotypes associated with the reduced processing of recombination intermediates caused by depleting SLX4 alone, suggesting that SLX4 and MutSβ also collaborate *in vivo* (26).

In this study, we undertook a detailed analysis of the interaction between SLX4 and MSH2. We precisely characterise the SLX4–MSH2 binding interface in both proteins. We show that it involves the association between an MSH2-interacting peptide (SHIP box) that we found in the N-terminus of SLX4 and the so-called lever 1 domain of MSH2. Furthermore, we find that SLX4 can interact with both MutSβ and MutSα. Cellular functional analyses exploiting a CRISPR-Cas9-engineered cell line that produces an N-terminally truncated SLX4 protein reveal that whilst the SLX4–MSH2 interaction does not contribute to the function of SLX4 in ICL repair, it dampens the MutSα-dependent MMR activity *in vivo* and *in vitro*.

MATERIALS AND METHODS

Cell lines generation

HeLa Flp-In T-REx (HeLa FITo: parental cells, kindly provided by Stephen Taylor) were maintained in DMEM, 10% FBS, Pen/strep (Gibco) + 4 μg/ml Blasticidin (Invivogen). In order to knock-out *SLX4* gene in these cells, we used a CRISPR-Cas9 approach with commercially available plasmids from Santa Cruz Biotechnology (sc-404395 and sc-404395-HDR) allowing the insertion of an exogenous plasmid conferring Puromycin resistance at the endogenous *SLX4* locus. Cells were subsequently selected by 0.8 μg/ml Puromycin (InvivoGen) and individual resistant clones were isolated and tested for MMC sensitivity and Western blotting to detect SLX4. Several MMC hypersensitive clones were selected but only one (KO30) initially showed an apparent knock-out of SLX4 by western blot while the others displayed SLX4 forms with molecular weights (MW) distinct from WT SLX4. Although KO30 also presented a lower MW form of SLX4 in subsequent experiments, this clone was further studied and complemented with FLAG-HA (FHA)-tagged forms of SLX4 WT, UBZ-mutated or lacking the MSH2 binding domain (ΔMSH2bd) using the Flp-In system by co-transfecting them with pDEST-FRT-TO-FHA-SLX4 vectors and the POG44 plasmid (encoding the Flp recombinase). Recombinant clones were selected with 120 μg/ml Hygromycin (Invitrogen) and pooled to obtain a stable population maintained in medium containing Puromycin, Blasticidin and Hygromycin.

Mutagenesis, cloning and molecular biology

Site-directed mutagenesis for the generation of $SLX4^{\Delta MSH2bd}$ was achieved using the following primers: Fwd 5′ GCAGACCCCGAGCGTTTGAGAC 3′ and Rev 5′ CAATTGTGCTGTGCGGGGTTTG 3′. pENTR1A SLX4 WT was used as a template and PCR was performed with the Advantage HD polymerase (Clontech). The PCR product was then digested by DpnI and subsequently phosphorylated and ligated using T4 PNK and T4 ligase (NEB) before transformation of *E. coli* DH5α. Clones harboured the expected loss of one AvaII restriction site and the SLX4 insert of one clone was fully sequenced. A gateway LR reaction was then performed to get the pDEST-FRT-TO-FHA and pDEST-FRT-TO-YFP expression vectors of $SLX4^{\Delta MSH2bd}$.

All the MSH2 constructs and the M453I mutant were obtained through gene synthesis or mutagenesis and cloned in pcDNA3.1(+)-N-eGFP by GenScript. These MSH2 constructs contain a N-terminal SV40 NLS to achieve nuclear localization.

Genomic DNA extraction using 4×10^6 HeLa FITo or HeLa KO30 cells was performed using the DNeasy Blood & Tissue Kit (Qiagen). PCR was performed on 100 ng genomic DNA using PrimeStar GXL SP DNA polymerase (Takara Bio RF220Q) to check exon 3 integrity and plasmid insertion using the following primers:

- Fwd: 5′ AGGAGCTGACAGAGCAGAGG 3′
- Rev: 5′ TGAGGTGCTGTTGTCATGGT 3′
- Fwd^{PURO}: 5′ GCAACCTCCCCTTCTACGAGC 3′

Antibodies and western blot

SDS-PAGE and western blotting were performed using a Novex NuPAGE SDS-PAGE Gel System and XCell II blot module (Invitrogen). Hybond-C Extra membrane (RPN203E) was purchased from GE healthcare. ECL Prime (RPN2236) or ECL Select (RPN2235) WB Detection Reagents were from Cytiva. A Chemidoc MP imaging system (Biorad) was used for signal detection. PageRuler Plus Prestained Protein Ladder (Thermo Scientific), Amersham ECL Rainbow Marker (Cytiva) or Color-coded Prestained Protein Marker (Cell Signaling Technology) were used as molecular weight standards.

Primary antibodies against SLX4 (A302-270A, A302-269A), EXO1 (A302-640A), MSH6 (A300-022A), MSH3

(A305-314A), pS4-S8 RPA32 (A300-245A) and SMC3 (A300-060A) were purchased from Bethyl laboratories. MSH2 (ab70270) and RPA32 (ab2175) antibodies were from Abcam. Anti-MSH2 (3A2 #2850), anti-MSH6 (3E1 #12988), anti-p345CHK1 (133D3 #2348) and anti-p68CHK2 (C13C1 #2197) were from Cell Signaling Technology. Anti-XPF (AM00551PU-N) was from Acris. FANCD2 (sc-20022), CHK1 (sc-8408) and PCNA (sc-56) antibodies were purchased from Santa Cruz Biotechnology. Anti-FLAG (F3165) and anti-GFP (JL-8) were from Sigma and Clontech, respectively. Anti-RPA70 (NA13) was purchased from Calbiochem.

The following secondary antibodies were purchased from Dako: goat anti-rabbit immunoglobulin G (IgG)/horseradish peroxidase (HRP) (P0448), goat anti-mouse IgG/HRP (P0447) and rabbit anti-goat IgG/HRP (P0449). To avoid the signal of the IgG used for immunoprecipitation, specific secondary antibodies were eventually used in IP/WB experiments (Veriblot, Abcam).

Transient transfections and co-immunoprecipitation

HeLa cells were transfected with lipofectamine 2000 (Invitrogen) or polyethylenimine (PEI, gift from Mauro Modesti). If needed, overexpression of FHA-SLX4 was typically achieved with 100 ng/ml of doxycycline (Sigma). Cells were harvested 24 h after transfection and the pellet was usually frozen for at least one night at -80°C. Frozen pellets were lysed in NETN buffer (50 mM Tris–HCl [pH 8.0], 150 mM NaCl, 1 mM EDTA, 0.5% [v/v] NP-40 supplemented with Complete EDTA-free protease inhibitor cocktail (Roche)) with rotation at 4°C before sonication and clarification by centrifugation. Immunoprecipitations (IPs) were performed overnight at 4°C with anti-FLAG M2 beads (Sigma), GFP trap (Chromotek) or anti-SLX4 (Bethyl, A302-269A and/or A302-270A) and control rabbit IgG (Cell Signaling, 2729S) coupled to dynabeads-protein G (Invitrogen). Beads were extensively washed with NETN buffer before elution in loading buffer.

For immunoprecipitation on solubilized chromatin, HeLa FITo cell pellets (3×10^7 cells) were resuspended in 1 ml of solution A (10 mM HEPES at pH 7.9, 10 mM KCl, 1.5 mM $MgCl_2$, 0.34 M sucrose, 10% glycerol, 1 mM DTT and protease inhibitors). After addition of Triton X-100 to a final concentration of 0.1%, cells were incubated on ice for 5 min before low-speed centrifugation (1300g for 4 min at 4°C). The nuclei pellet was washed once with solution A before lysis in 1 ml of nuclease buffer (50 mM Tris–HCl [pH 8], 100 mM NaCl, 4 mM $MgCl_2$, 0,5% NP-40 and protease inhibitors) for 40 min with rotation at 4°C. After high-speed centrifugation (21 000g for 30 min at 4°C), the supernatant representing the nuclear soluble fraction was taken. The pellet was resuspended in 1 ml of nuclease buffer and after a brief sonication, 4 μl of Pierce universal nuclease (Thermo Scientific) was added and the mixture was incubated at RT for 30 min. After another brief sonication, 2 μl of Pierce universal nuclease was added again before incubation at RT for an additional 10 min. After high-speed centrifugation at 4°C for 20 min, the supernatant representing the chromatin fraction was taken. Nuclear soluble and chromatin fractions were further used in IP as described before except that nuclease buffer was used for IP washes

siRNA

Cells were transfected with the following siRNA at a concentration of 5 nM using INTERFERin (Polyplus transfection):

- siLUC (CGUACGCGGAAUACUUCGA*dTdT*)
- siMSH2 (AAUCUGCAGAGUGUUGUGCUU*dTdT*) [from (35)]
- siSLX4-1 is a mix of two siRNA targeting the UTRs of SLX4: SLX4 UTR87 (GCACCAGGUUCAUAUGUAU*dTdT*) and SLX4 UTR7062 (GCACAAGGGCCCAGAACAA*dTdT*),
- siSLX4-2 is a pool of siRNA synthetized by Dharmacon (M-014895–01-0005)
- siSLX4-3 (AAACGUGAAUGAAGCAGAA*UU*) [from (3)]
- siSLX4-4 (CAGATCTCAGAAATCTTCATCCAAA) is a Stealth siRNA synthetized from Invitrogen.

Unless otherwise specified, siRNAs were purchased from Eurofins MWG Operon.

Clonogenic survival assay

Cell lines (HeLa FITo, KO30, KO30 + WT, KO30+ΔMSH2bd, KO30 + UBZ^{mut}) were seeded at low density (450–500 cells) in 60 mm Petri dishes. Moderate expression of exogenous FHA-SLX4 was achieved by addition of 2 ng/ml of doxycycline throughout the entire experiment. For siRNA treatment, cells were transfected the day before at 5 nM siRNA in six-well plates before low density seeding. Genotoxic treatments with mitomycin C, melphalan, 6-thioguanine or *N*-methyl-*N*'-nitro-*N*-nitrosoguanidine (Sigma) were performed the next day for 24 h before drug retrieval, PBS wash and addition of fresh medium. Cells were usually fixed and stained 7–8 days later when visible colonies could be counted with a Scan 1200 automatic colony counter (Interscience).

Peptide pulldown

To prepare nuclear extracts for the pulldown, frozen HeLa FITo cell pellets were resuspended in solution A (10 mM HEPES at pH 7.9, 10 mM KCl, 1.5 mM $MgCl_2$, 0.34 M sucrose, 10% glycerol, 1 mM DTT and protease inhibitors). After addition of Triton X-100 to a final concentration of 0.1%, cells were incubated on ice for 10 min before low-speed centrifugation (1300g for 4 min at 4°C). The resulting nuclei pellet was washed once with solution A before lysis in extract buffer (50 mM HEPES, pH 7.3; 150 mM NaCl; 10% sucrose supplemented with protease inhibitors) and incubated with rotation for 1 h at 4°C including one round of sonication. Pre-washed streptavidin magnetic beads (Genscript) were added for an additional 30 min and nuclear extracts were subsequently clarified by high-speed centrifugation. Protein concentration was measured using Pierce 660 nm Protein Assay Reagent.

WT and mutant SLX4 peptides were synthetized by Genscript and resuspended in H_2O. Peptides (20 μg) were immobilized on pre-washed streptavidin magnetic beads (Genscript) in TBS with 1% BSA for 1 h at RT before washes in TBS to get rid of unbound peptides and resuspension in extract buffer without NaCl in order to get a final molarity of 110 mM NaCl for the pulldown. Beads were incubated with nuclear extracts (425 μg) for 1 h 15 at 4°C, washed 4 times in extract buffer (110 mM NaCl) before elution in loading buffer.

Nuclear extracts for *in vitro* MMR assay

Nuclear extracts preparation was essentially performed according to a published protocol with minor modifications (36). Briefly, 1–2 × 10^8 HeLa FITo cells were collected, washed with PBS and resuspended in 12 ml of cold hypotonic buffer (20 mM HEPES, pH 7.3; 0.2M sucrose; 5 mM KCl; 0.5 mM $MgCl_2$; 0.5 mM PMSF; 2 mM DTT and supplemented with Complete EDTA-free protease inhibitor cocktail (Roche)). Cells were pelleted at 2000g for 5 min at 4°C, resuspended in 4 ml of hypotonic buffer without sucrose and incubated on ice for 10 min. After 10 strokes of Dounce homogenizer (loose-fitting), the solution was centrifuged at 2000g for 5 min at 4°C. The nuclear pellet was lysed in 1 ml of extract buffer (50 mM HEPES, pH 7.3; 10% sucrose; 0.5 mM PMSF; 2 mM DTT and supplemented with Complete EDTA-free protease inhibitor Cocktail). NaCl was added and adjusted to 150 mM before incubation with rotation at 4°C for 1 h. The nuclear suspension was centrifugated for 30 min at 15 000g and supernatant was concentrated using Vivaspin 6 (10 kDa MWCO) centrifugal concentrator (Sartorius). Aliquots of concentrated nuclear extracts were frozen in liquid nitrogen and stored at −80°C.

Construction of the mismatched DNA substrate

For this study, we exploited a previously published plasmid construction (pLL1/2c) that contains a G/T mismatch in a *Pvu*II unique site (37). In order to introduce a nick downstream the G/T mismatch, pLL1 and pLL2c plasmids were modified by site-directed mutagenesis to introduce a *Bbv*CI restriction site 132bp far from the mismatch. The new plasmids were renamed pLL104 and pLL105. The mismatched DNA substrate was obtained following the gap-duplex method (38) using 200 μg of pLL104 and pLL105 and a 17mer oligo (GCAAGAATATTAACACG) that allows to ligate only the gap-duplex form we are interested in. Subsequently the DNA substrate was purified by CsCl/ethidium bromide gradient, recovered under UV light and resuspended in TE. Quantification on agarose gel estimated the final yield around 4–6 μg.

In vitro MMR assay

To create a 5′ nick downstream the G/T mismatch, 2 μg of the DNA substrate were digested with 30 U of Nb.BbvCI (from NEB) for 2 h at 37°C. Some linear by-product was observed together with the nicked DNA due to random nicks caused by exposure to UV light. To eliminate the linear DNA we digested with 40 U ExoV (from NEB) for 1 h at 37°C. The nicked DNA substrate was finally extracted by phenol-chloroform followed by ethanol acetate precipitation and resuspended in TE to a final concentration of 40 ng/μl.

In vitro MMR assays were performed with minor modification as previously described (36): 80 ng of nicked DNA substrate were added to 50 μg of nuclear extract in a 50 μl final volume. MMR buffer was as followed: 0.1 mM each of four dNTPs, 20 mM Tris–HCl pH 7.6; 1.5 mM ATP; 1 mM glutathione; 5 mM $MgCl_2$; 50 μg/ml BSA; the salt concentration was adjusted to 110 mM NaCl. SLX4 peptides were eventually added to the reaction at the indicated concentration. After incubation at 37°C for 30 min, the reaction was terminated by the addition of 100 μl of stop solution (25 mM EDTA, 0.67% sodium dodecyl sulfate, and 300 μg/ml proteinase K), then incubated at 37°C for another 15 min. DNA was extracted twice with an equal volume of phenol/chloroform and once with chloroform, precipitated by ethanol/acetate and resuspended in 10 μl H_2O. To analyze the repair of the mismatch, the DNA substrates were digested with 10U of ApaLI and PvuII-HF for 1 h at 37°C (RNase was added 20min before the end of the incubation) and visualized on a 1% agarose gel. ImageJ software was used for quantification.

RESULTS

SLX4 associates with both MutSα and MutSβ

In agreement with previous reports (3,33), we detected by Western blot (WB) endogenous MSH2 in SLX4 immunoprecipitates (IP) performed on whole cell extracts from HeLa Flp-In T-REx (FITo) cells transiently transfected with a FLAG-HA-SLX4 (FHA-SLX4) expression vector (Figure 1A). In contrast, we were unable to detect MSH2 when we immunoprecipitated endogenous SLX4 (Figure 1B), suggesting that only a minor fraction of SLX4 is in complex with MSH2. Using mass spectrometry as a complementary approach, we specifically identified MSH2 and MSH6 peptides in endogenous SLX4 immunoprecipitates (Supplementary Figure S1A), supporting endogenous SLX4-MutSα complex formation. We suspected that our difficulty to readily detect an interaction between endogenous SLX4 and MSH2 in whole cell extracts might be due to a weak and/or transient interaction and/or that it occurs preferentially on chromatin. In agreement, we found that the relative co-IP of MSH2, MSH6 and MSH3 with endogenous SLX4 was enhanced in a chromatin fraction compared to a nuclear soluble fraction (Figure 1C). Our results thereby demonstrate that MutSα and MutSβ complexes are *bona fide* partners of endogenous SLX4.

Identification of the MSH2-binding domain in SLX4

MSH2 was initially shown to interact with a fairly large N-terminal SLX4 fragment (aa 1–669) (3). As shown in (Supplementary Figure S1B), we tested the ability of several shorter FLAG-tagged N-terminal fragments of SLX4 to co-immunoprecipitate MSH2 when over-expressed in HeLa cells. A FLAG-SLX4$^{1\text{-}381aa}$ fragment was sufficient to pull-down MSH2 (Supplementary Figure S1B). In contrast, we were unable to co-immunoprecipitate MSH2 with a shorter

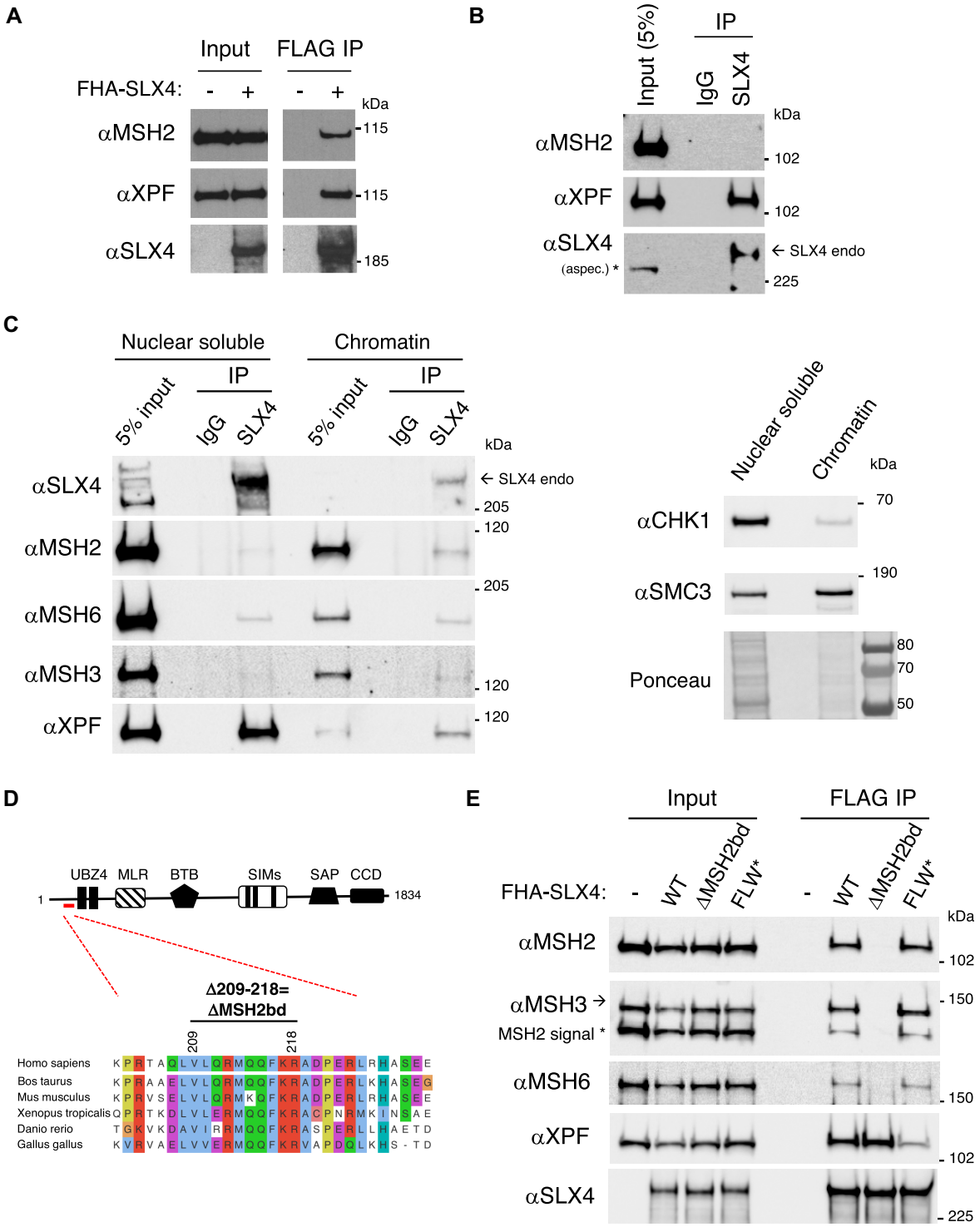

Figure 1. SLX4 interacts with both MutSα and MutSβ through a conserved N-terminal region. (**A**) HeLa FITo cells were transfected with FLAG-HA-SLX4 (FHA-SLX4) vector before FLAG immunoprecipitation (IP) and western blotting, which shows that MSH2 co-immunoprecipitates with overexpressed SLX4. (**B**) IP of endogenous SLX4. Co-immunoprecipitation (coIP) of MSH2 with endogenous SLX4 is barely detectable compared to experiments using overexpressed FHA-SLX4 as in A. The asterisk indicates an aspecific band recognized by the anti-SLX4 antibody (**C**) Left panel: IP of endogenous SLX4 from a nuclear soluble fraction or a chromatin-solubilized fraction in which the coIP of MSH2, MSH3 and MSH6 is readily detected. Right panel: control of the fractionation by western blot against CHK1, mainly nuclear soluble, and SMC3 enriched in chromatin. (**D**) Scheme of SLX4 illustrating the location and conservation of a short domain representing the putative MSH2 binding domain (MSH2bd) deleted in SLX4$^{\Delta MSH2bd}$. Alignments were performed with ProViz (81). (**E**) HeLa FITo cells were transfected with FHA-SLX4 WT, FHA-SLX4$^{\Delta MSH2bd}$ or FHA-SLX4^{FLW*}, which is deficient for XPF binding, before FLAG IP and western blotting with the indicated antibodies.

internal FLAG-SLX4$^{340\text{-}580aa}$ fragment, which readily interacts with XPF. This indicates that the MSH2 binding domain is located between residues 1 and 381 and that critical residues for MSH2 binding are located before residue 340. The well-described tandem UBZ4 domains of SLX4 as well as other evolutionary conserved domains of unknown function are located in between residues 1 and 380. A contribution of the UBZ motifs to MSH2 binding could be excluded as an over-expressed YFP-SLX4^{UBZ} mutant protein interacted with MSH2 as well as the YFP-SLX4 wild type control (Supplementary Figure S1C). In contrast, a small 10 aa deletion (Δ209–218) within one of the short conserved domains found in the N-terminus of SLX4 (Figure 1D) totally abrogated interaction with MSH2, MSH3 and MSH6, but not XPF (Figure 1E). These data indicate that this conserved motif is an essential part of the MSH2 binding domain (MSH2bd) and we will refer hereafter to the SLX4 mutant lacking residues 209–218 as the SLX4$^{\Delta MSH2bd}$ mutant.

Lever 1 domain of MSH2 is required for SLX4 binding

We next undertook experiments to delineate the SLX4-interacting region of MSH2. For this, we overexpressed and immunoprecipitated several deletion constructs of GFP-tagged MSH2 (Supplementary Figure S1D). An MSH2$^{1–460aa}$ N-terminal fragment that contains the so-called lever 1 domain was sufficient to pull-down SLX4 but not MSH3 and MSH6. In contrast, a shorter MSH2$^{1–310aa}$ fragment lacking the lever 1 domain was unable to interact with SLX4 (Supplementary Figure S1D), demonstrating that the lever 1 domain of MSH2 is critical for interaction with SLX4. However, these data also suggest a contribution of MSH2 lever 2 domain in stabilizing SLX4 interaction as fragments lacking the lever 2 (MSH2$^{1–550aa}$ and MSH2$^{1–460aa}$) interacted less with SLX4 than full length MSH2. As SLX4–MSH2 complex formation can occur independently of MSH3 and MSH6, these results also strengthen the fact that it is the SLX4–MSH2 direct interaction that drives interaction with MutSα and MutSβ.

Generation and characterization of an N-terminal truncated SLX4 cellular model

In order to determine the functional significance of the SLX4–MSH2 interaction, we took advantage of an N-terminally truncated SLX4 mutant HeLa cell line that we generated by CRISPR-Cas9-based genome editing of HeLa FITo cells. Using a strategy designed to knock-out *SLX4 via* the insertion of a Puromycin-resistant cassette in the first exons of the *SLX4* gene by CRISPR-Cas9 and HR, we retrieved several clones harbouring a severe MMC hypersensitivity, which is indicative of loss of SLX4 functions (Supplementary Figure S2A and Supplementary Figure S2B). However, WB analyses with an anti-SLX4 antibody revealed bands at unexpected molecular weights (MW) in these clones, in particular a recurrent lower MW SLX4 signal (Figure 2A, Supplementary Figure S2C and Supplementary Figure S2D). Analysis of two of these clones (clones KO1 and KO30) showed that this signal revealed by an antibody directed against the SLX4 C-terminus is lost following SLX4 depletion by siRNA (Figure 2A). This strongly suggested that clones KO1 and KO30 produce an N-terminally truncated protein (termed SLX4ΔNter), consistent with our genome editing strategy that targeted the first exons of the *SLX4* gene. Using a combinatorial approach, we further characterized the origin and nature of SLX4ΔNter in KO30 cells (for details, see Supplementary Results and Supplementary Figure S3A-H). Our data indicate that KO30 cells use an alternative translation initiation site to produce a shorter SLX4$^{360\text{-}1834aa}$ C-terminal variant that starts at Methionine 360, thus lacking the tandem UBZ4 and the MSH2bd (Figure 2B).

Loss of the SLX4 UBZ4 domains in KO30 cells is sufficient to explain their severe MMC hypersensitivity (Figure 2C) as the first UBZ4 motif is essential for the ICL repair function of SLX4 (10). We validated this new cellular model by complementing KO30 cells with exogenous FLAG-HA-(FHA)-tagged SLX4 WT or SLX4^{UBZ} mutant. As shown in Figure 2C, MMC hypersensitivity of KO30 cells was largely complemented by SLX4 WT but not at all by SLX4^{UBZ}, establishing our KO30 cells as a worthwhile model for cellular complementation experiments aimed at studying SLX4 functions that rely on its first 359 residues.

The SLX4–MSH2 interaction is NOT required for ICL resistance

Besides the loss of the UBZ4 domains, we could not rule out that the concomitant loss of the MSH2-binding domain in KO30 cells might also contribute to their MMC hypersensitivity since earlier studies showed that MSH2 deficiency is also associated with hypersensitivity to various ICL-inducing agents (39–41). We thus evaluated a possible interplay between MSH2 and SLX4 in ICL repair. In agreement, MSH2 depletion sensitized HeLa cells to MMC (Figure 3A and Supplementary Figure S4A). We next investigated whether this function of MSH2 in ICL repair was dependent on its interaction with SLX4 by complementing KO30 cells with the SLX4$^{\Delta MSH2bd}$ mutant. Of note, this mutant appeared to be expressed in KO30 cells at lower levels than the WT protein in two independent complementation experiments (Figure 3B and data not shown). Nevertheless, SLX4$^{\Delta MSH2bd}$ could restore MMC resistance of KO30 cells as well as SLX4 WT (Figure 3C), indicating that the role of MSH2 in ICL repair is independent of SLX4. To strengthen these findings, we assessed whether the MSH2-SLX4 interaction contributed to a structurally distinct ICL induced by Melphalan (42). We observed similar complementation levels of the marked sensitivity of KO30 cells to Melphalan with both SLX4 WT and SLX4$^{\Delta MSH2bd}$ (Figure 3D and Supplementary Figure S4B). Based on these data we conclude that SLX4–MSH2 complex formation is not required for ICL repair.

The SLX4–MSH2 interaction confers resistance to 6-TG and MNNG: Is SLX4 an inhibitor of MutSα ?

As the SLX4–MSH2 interaction turned out to be dispensable for the essential role of SLX4 in ICL repair, we next tested whether SLX4 was involved in a canonical MMR function. One of the hallmarks of the majority of MMR-defective cells is their resistance to the cytotoxic effects

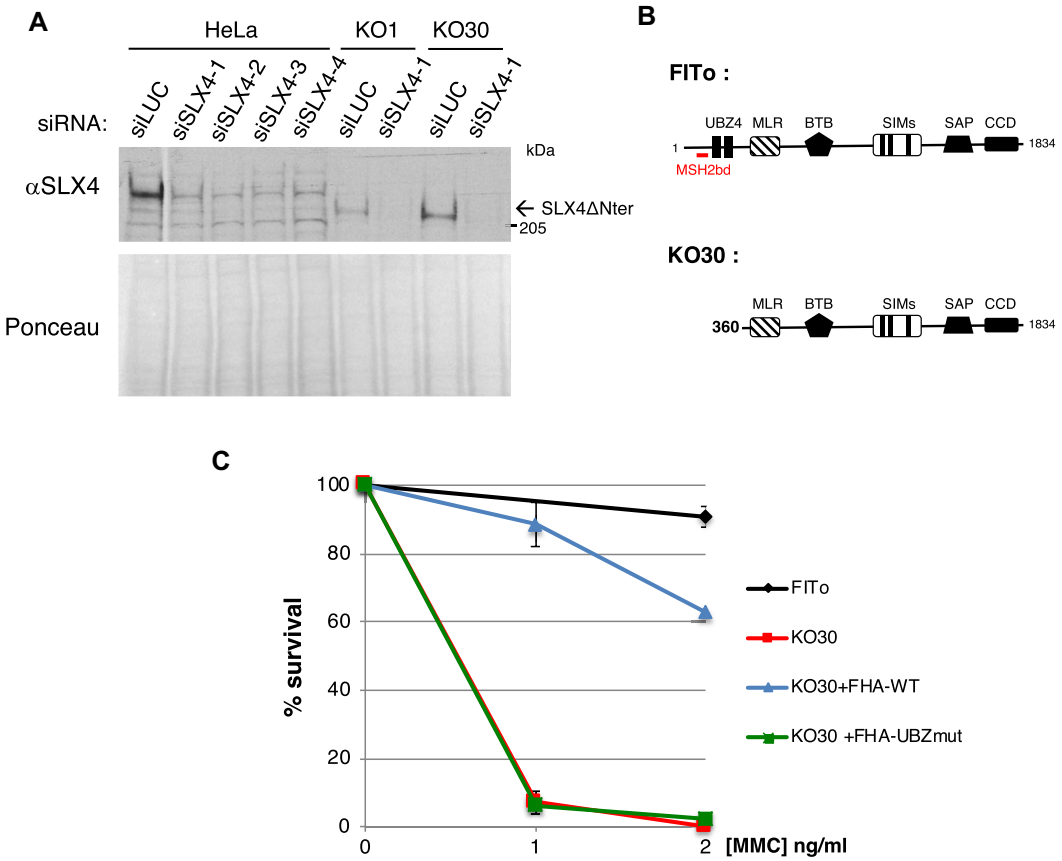

Figure 2. Characterization of the KO30 cell line expressing an N-terminally truncated form of SLX4. (**A**) Western blot showing that HeLa FITo KO1 and KO30 clones generated by CRISPR-Cas9 express a truncated form of SLX4 termed SLX4ΔNter (indicated by an arrow), the expression of which is sensitive to a siRNA that targets *SLX4* mRNA. (**B**) SLX4ΔNter protein starts at Methionine 360; see supplementary results for details. (**C**) Clonogenic survival assay in response to mitomycin C (MMC) of HeLa FITo, KO30 cells and KO30 cells complemented with FHA-SLX4 WT or UBZ-mutated (UBZmut). Cells were treated for 24 h with the indicated dose of MMC ($n = 2$–4 experiments, mean ± SD are represented).

of the long used anti-tumoral drug 6-thioguanine (6-TG). This purine analogue is a pro-drug requiring metabolic activation before incorporation into DNA during replication. Once incorporated, a methylation step generates the S^6-methylthioguanine (S^6-MeTG) that can readily mispair with a Thymidine (T) during the next round of replication. Perceived as a replication error, the S^6-MeTG:T mismatch is recognized by MutSα (MSH2-MSH6) followed by the excision of the newly incorporated T. A new erroneous incorporation of a T in the daughter strand can then result in futile MMR activity leading to persistent DNA breaks and cell death (43). To assess whether SLX4–MSH2 complex formation contributes to MMR, we monitored cellular sensitivity to 6-TG of both SLX4-depleted cells and the KO30 cell line that produces N-terminally truncated SLX4 that does not bind MSH2. As expected, MSH2-depleted cells were resistant to 6-TG (Figure 4A). In contrast, SLX4 depletion significantly sensitized cells to 6-TG (Figure 4A). Remarkably, KO30 cells also displayed hypersensitivity to 6-TG, which was suppressed by SLX4 WT but not by the $SLX4^{\Delta MSH2bd}$ mutant (Figure 4B). To substantiate our findings, we examined the response of KO30 cells complemented with SLX4 WT or $SLX4^{\Delta MSH2bd}$ after exposure to the methylating agent *N*-methyl-*N*'-nitro-N-nitrosoguanidine (MNNG). MNNG produces distinct DNA lesions but its toxicity is mainly ascribed to the generation of O^6-methylguanine (^{6Me}G), which can mispair with a thymidine and induce a cytotoxic MMR-dependent response in a similar way to 6-TG. As shown in Figure 4C, KO30 cells expressing $SLX4^{\Delta MSH2bd}$ were markedly more sensitive to MNNG compared to cells expressing SLX4 WT (Figure 4C). As MMR-mediated processing of ^{6Me}G induces a checkpoint response following moderate doses of MNNG (44,45), we examined markers of checkpoint activation in our experimental set-up. We found that phosphorylation of CHK1, CHK2 and hyperphosphorylation of RPA32 were more pronounced and persistent after MNNG treatment in KO30 cells expressing $SLX4^{\Delta MSH2bd}$ compared to those expressing SLX4 WT (Figure 4D). Thus, loss of interaction between SLX4 and MSH2 appears to enhance the activity of MMR. Taken together, our results demonstrate that SLX4 does not positively contribute to MMR but rather negatively impacts the repair process via its interaction with MSH2, thereby protecting cells against the MMR-mediated 6-TG and MNNG toxicity.

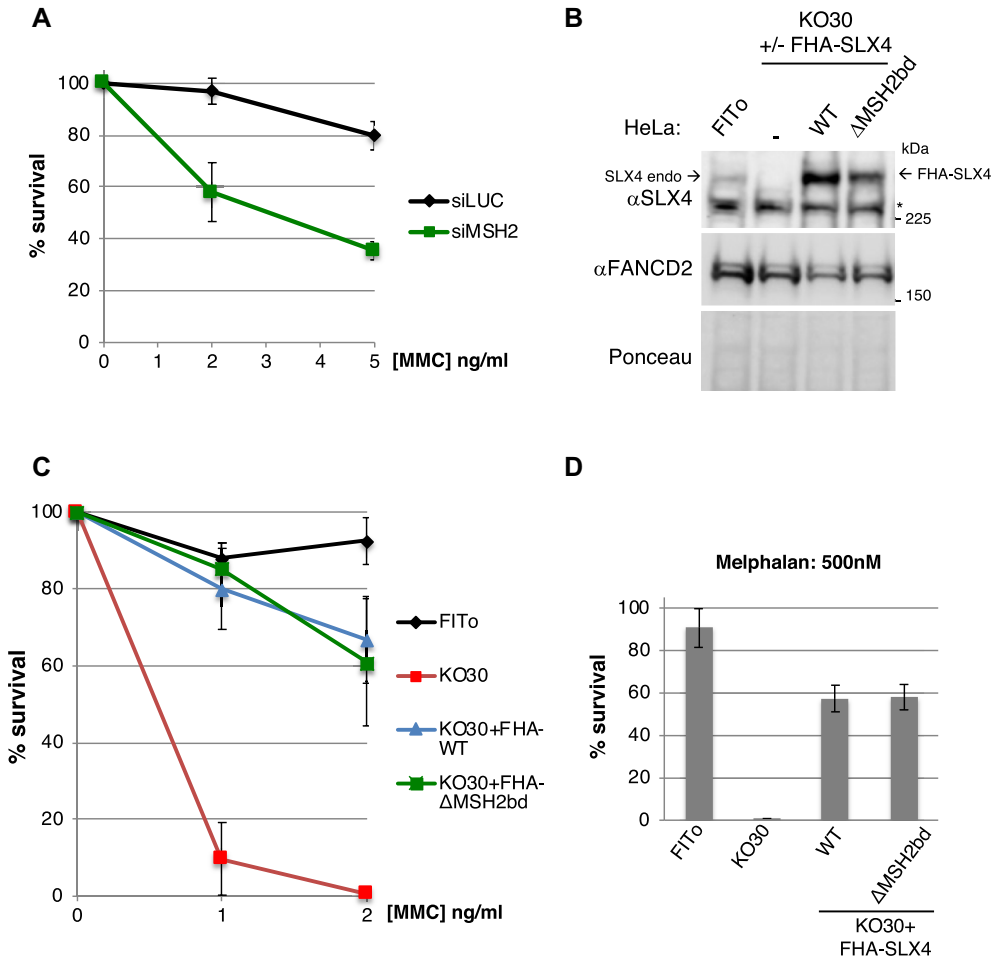

Figure 3. Interaction of MSH2 and SLX4 is not required for ICL repair. (**A**) Clonogenic survival assay in response to MMC of HeLa FITo cells transfected with control siRNA (siLUC) or siRNA targeting MSH2 (siMSH2) ($n = 3$ for MMC 2 ng/ml, $n = 4$ for MMC 5 ng/ml, mean ± SEM are represented on the graph). (**B**) Complementation of KO30 cells with FHA-SLX4 WT or SLX4$^{\Delta MSH2bd}$. Induction of exogenous SLX4 expression was achieved with 2 ng/ml of doxycycline as in (C) and (D). (**C**) Clonogenic survival assay of HeLa FITo, KO30 cells and KO30 cells complemented with FHA-SLX4 WT or SLX4$^{\Delta MSH2bd}$ in response to MMC ($n = 3$ for MMC 1 ng/ml, $n = 5$ or 6 for MMC 2 ng/ml, mean ± SD are represented). (**D**) Same as in (C) except that Melphalan (500 nM) was used as an alternative crosslinking agent ($n = 3$, mean ± SD are indicated).

SLX4 negatively regulates MMR through a SHIP box-mediated interaction with MSH2

To help better understand how SLX4 may negatively impact MMR through direct binding to MSH2, we further analysed the MSH2bd *in silico*. We noticed some degree of conservation, albeit moderate, with the previously described SHIP (Msh2-interacting peptide) boxes of *Saccharomyces cerevisiae* Exo1 that drive interaction with Msh2 (46) (Figure 5A). These motifs, two of which are found in the C-terminus of Exo1, have also been found in other yeast proteins (46). Mutating Methionine M470 of Msh2 into Isoleucine (Msh2^{M470I}) disrupts its interaction with SHIP-box containing proteins (46). The conserved *S. cerevisiae* Msh2 M470 residue corresponds to the human MSH2 M453 residue (Supplementary Figure S5A), which is located in an exposed helix (47) compatible with protein–protein interactions (Supplementary Figure S5B) at the end of the lever 1 domain of MSH2 required for binding to SLX4 (Supplementary Figure S1D). Remarkably, as shown in Figure 5B, introducing the M453I mutation in MSH2 not only severely impacted interaction with EXO1, it also disrupted complex formation with SLX4 (Figure 5B). Our data suggest that the SHIP-box-mediated Msh2-Exo1 interaction, initially identified in *S. cerevisiae*, is conserved throughout evolution and that the MSH2bd of SLX4 is a *bona fide* SHIP box.

To definitely establish that the MSH2 binding domain is a SHIP box, we performed peptide pulldown assays using biotinylated peptides of SLX4 containing a WT or mutated SHIP box (Figure 5C). While endogenous MSH2 was readily pulled-down with the SLX4 WT peptide, mutation of the most conserved aromatic residue within SHIP boxes (46) (F216 in SLX4) was sufficient to disrupt MSH2 binding (Figure 5C) confirming that SLX4 interacts with MSH2 through a SHIP box. Finally, we investigated the ability of the SLX4 SHIP box peptide to inhibit MMR *in vitro* using a well-established assay in which a substrate containing a G–T mismatch and a 5′ nick is incubated with HeLa nuclear extracts and repair of the mismatch visualized by the restoration of a functional PvuII restriction site (Figure 5D

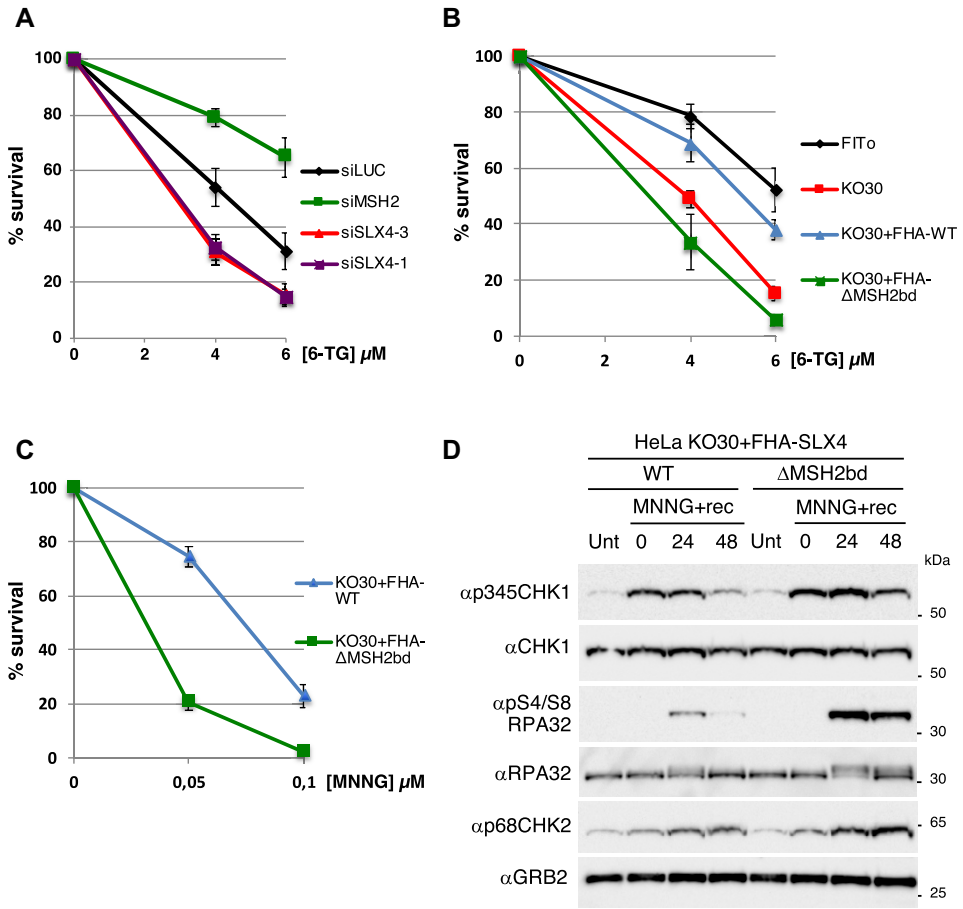

Figure 4. Interaction of SLX4 and MSH2 contributes to the toxicity of 6-thioguanine (6-TG) or N-methyl-N'-nitro-N-nitrosoguanidine (MNNG). (**A**) Clonogenic survival assay of HeLa FITo cells transfected with the indicated siRNA in response to a 24 h treatment with 6-TG ($n = 4$–7 experiments, mean ± SEM are represented). (**B**) Clonogenic survival assay in response to 6-TG of HeLa FITo, KO30 cells and KO30 cells complemented with FHA-SLX4 WT or SLX4$^{\Delta MSH2bd}$ ($n = 3$–5 experiments, mean ± SEM are represented). (**C**) Clonogenic survival assay in response to MNNG of KO30 cells complemented with FHA-SLX4 WT or SLX4$^{\Delta MSH2bd}$ ($n = 3$–4 experiments, mean ± SEM are represented). (**D**) KO30 cells complemented with FHA-SLX4 WT or SLX4$^{\Delta MSH2bd}$ were treated with MNNG (0.1 μM) for 24 h before drug removal and addition of fresh medium. Cells were collected at the indicated time points of recovery (+rec) and induction of the DNA damage response was analysed by western blot.

and Supplementary Figure S5C) (36). Strikingly, addition of an excess of the SLX4 SHIP box peptide virtually abrogated mismatch repair while mutant peptides had barely any effect (Figure 5D). Titration analysis revealed that a 10 μM concentration of SLX4 SHIP peptide was sufficient to strongly inhibit the MMR reaction (Supplementary Figure S5D). Overall, our data demonstrate that the SHIP box of SLX4 can inhibit MutSα-dependent MMR both *in vivo* and *in vitro* through direct interaction with MSH2.

DISCUSSION

In this study, we have characterized the mode of interaction between SLX4 and MSH2 and investigated its functional relevance. We demonstrate that the interaction of SLX4 with MSH2 relies on a short conserved motif located upstream of the first UBZ4 domain of vertebrate SLX4 proteins. This motif resembles the small SHIP box motif previously identified in partners of *S. cerevisiae* Msh2 (46). It was previously shown that the SHIP box-mediated interaction requires the integrity of the M470 residue of yeast Msh2 (46). Importantly, we show that mutating the equivalent M453 residue at the end of the lever 1 domain in human MSH2 (MSH2^{M453I}) strongly affects the association of MSH2 with EXO1 (Figure 5B) thereby confirming that the SHIP box-mediated interaction with MSH2 is conserved from yeast to human, as previously anticipated (46). Importantly, MSH2^{M453I} is also strongly impaired in complex formation with SLX4 (Figure 5B). Furthermore, a short deletion of 10 residues within the small conserved N-terminal motif of SLX4 that is required for MSH2 binding strongly impairs its association with both MutS complexes (Figure 1E) and a small peptide containing that motif is sufficient to pulldown MSH2 (Figure 5C). Our findings thus demonstrate that SLX4 contains a *bona fide* SHIP box that drives its interaction with MSH2.

The MutSα heterodimer (MSH2-MSH6), but not MutSβ (MSH2-MSH3), mediates the cytotoxicity of 6-TG and MNNG (48–51). The underlying mechanism is likely to involve futile cycles of MMR of meG-T mispairs (52), resulting in cell death. A 'direct signalling' model has also been proposed where MMR proteins directly activate ATR,

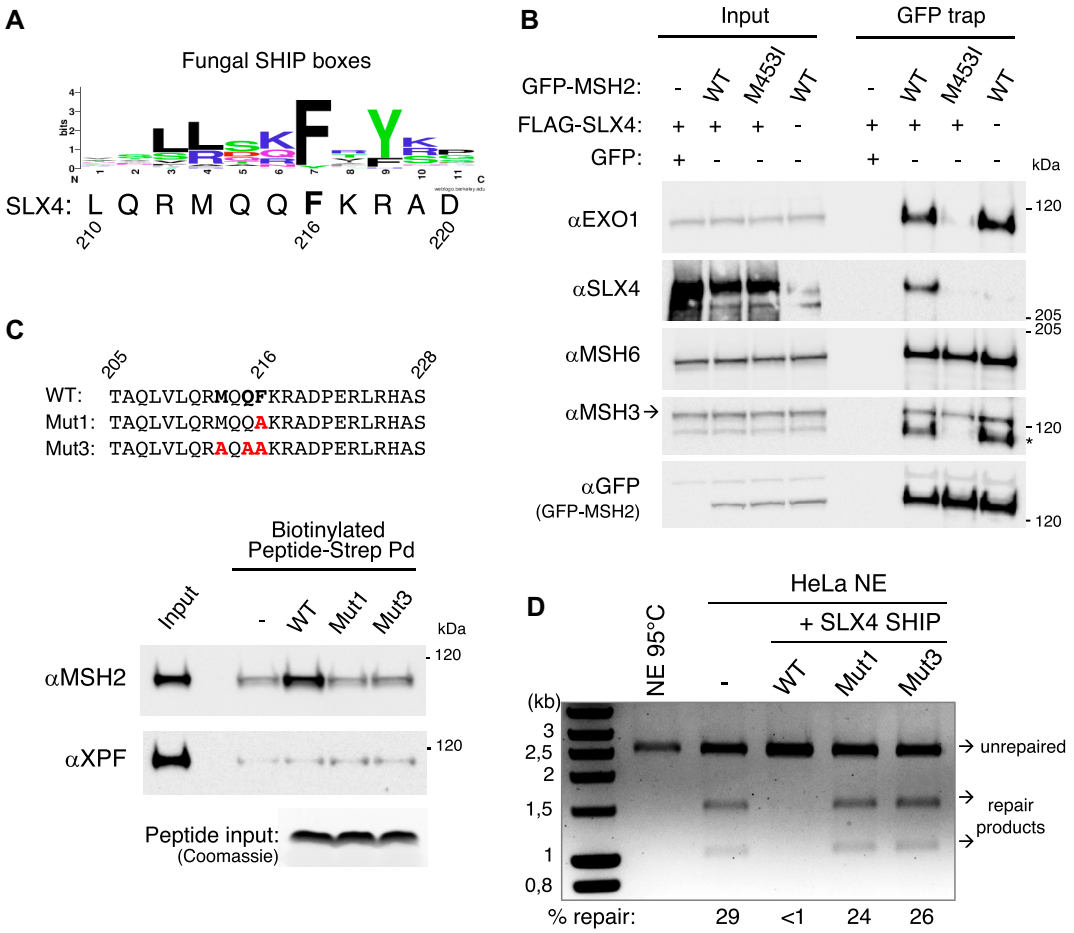

Figure 5. The MSH2 binding domain of SLX4 is a SHIP box that inhibits mismatch repair and antagonizes EXO1–MSH2 interaction. (**A**) Weblogo representation of multiple sequence alignments of SHIP boxes of Exo1 and Fun30 from fungal species in the *Saccharomycotina* (46,82). (**B**) HeLa FITo cells were transfected with expression vectors coding for GFP, FLAG-SLX4, GFP-MSH2 WT and/or GFP-MSH2^{M453I}, as indicated, before GFP pull-down and western blotting with the indicated antibodies. The asterisk represents the remaining signal for EXO1 when blotting for MSH3 after prior blotting for EXO1. (**C**) Peptide pull-down using biotinylated SLX4 peptides that contain a WT or mutated SHIP box, immobilized on Streptavidin-coated beads and incubated with HeLa nuclear extracts. Residues selected for mutagenesis are shown in bold in the WT sequence. (**D**) *In vitro* mismatch repair assay using a plasmid containing a G/T mismatch and a 5′ nick incubated with nuclear extracts (NE) from HeLa FITo cells as described in Material and Methods. Where indicated, WT or mutant SHIP peptides (80.5 μM) were added to the reaction. As a negative control, the NE was inactivated at 95°C before the reaction. DNA was purified and digested with ApaII and PvuII. Repair of the mismatch restores the PvuII site and produces two bands of 1.55 and 1.03 kb on an agarose gel. The percentage of repair is indicated.

without the need of processing the mismatch (53–55). These two models probably stand right and are not necessarily exclusive. In contrast to MSH2-depleted cells that gained expected 6-TG resistance, SLX4-depleted cells turned out to be hypersensitive to 6-TG (Figure 4). In agreement with our findings, an unbiased genome-wide CRISPR-Cas9 screen recently identified SLX4 as a determinant of MNNG resistance (56). Moreover, we demonstrated that the pro-survival role of SLX4 in response to 6-TG or MNNG is totally dependent on its interaction with MSH2 (Figure 4). This strongly suggests that SLX4 reduces MutSα-dependent MMR cytotoxic activity in response to these drugs. Besides inhibition of MMR, an alternative explanation for how SLX4 mediates 6-TG and MNNG resistance could have been through the resolution of HR intermediates formed after MutSα-dependent MMR. In line with this, cells lacking BRCA2 or RAD51 paralogs were previously shown to be hypersensitive to 6-TG or MNNG (57–60) and MutSβ stimulates *in vitro* the processing of HR intermediates by the SMX complex (26). However, MSH3-deficient cells are not sensitive to 6-TG nor MNNG making this an unlikely explanation (48–51).

How exactly SLX4 inhibits MutSα-dependent MMR is currently unclear. The identification of a SHIP box in SLX4 that mediates its interaction with MSH2 raises the possibility of a competition with other SHIP box containing proteins. Indeed, yeast Exo1 and Fun30 positively contribute to MMR via their SHIP boxes (46). In human cells, other proteins strongly suspected to interact with MSH2 via a SHIP box such as WDHD1/AND1/hCTF4, SMARCAD1 (Fun30 homolog) or MCM9 (46) are also positive regulators of MMR (61–64). Since SLX4 represents the first example of a SHIP box-containing protein that exerts an inhibition of MMR, as judged by 6-TG and MNNG toxicity analyses, it is tempting to speculate that it does so by competing with SHIP box-containing positive contrib-

utors. Amongst these, EXO1 is a strong candidate as it contributes to the cytotoxicity of 6-TG (65) and MNNG (66,67). In line with this, transient overexpression of FLAG-SLX4 decreased EXO1 interaction with GFP-MSH2 (Figure 5B). Moreover, we found that the interaction of GFP-MSH2 with endogenous EXO1 was slightly increased in KO30 cells compared to parental HeLa FITo cells (Supplementary Figure S5E). Similarly, enhanced interaction of EXO1 with GFP-MSH2 was observed in KO30 cells complemented with SLX4$^{\Delta MSH2bd}$ compared to cells complemented with SLX4 WT (Supplementary Figure S5F). Based on these observations we propose that SLX4 reduces the toxicity of 6-TG and MNNG, at least in part, by competing with EXO1 for MSH2 binding thereby limiting the rate of MMR and the associated futile cycle. In absence of SLX4 or when SLX4 cannot bind MSH2, an increased number of MMR transactions are taken to completion resulting in overall enhanced MMR activity and subsequent toxicity in response to 6-TG and MNNG. Bringing further support to this model, we showed that adding an excess of SLX4 SHIP box peptides to HeLa cell nuclear extracts abrogated 5′-directed repair of a G–T mismatch *in vitro* (Figure 5D). This peptide-based approach was initially used to demonstrate an early role of PCNA in MMR (preceding DNA resynthesis) using a p21 peptide containing a PCNA interacting protein (PIP)-box (68). The *S. cerevisiae* Exo1 SHIP1 box was also shown to inhibit MMR *in vitro* (46). Although these *in vitro* results obtained with the SLX4 SHIP box peptide are striking, the mechanism by which SLX4 mitigates MMR *in vivo* is certainly more complex. In line with this, we could not detect a significant difference in MMR activity between nuclear extracts from KO30 + SLX4 WT versus KO30 + SLX4$^{\Delta MSH2bd}$ cells (data not shown). A likely explanation is that our peptide-based experiment uses a vast excess of the SLX4 SHIP box peptide over EXO1 that will disrupt the EXO1-MSH2 interaction whereas the concentration of SLX4 in nuclear extracts, even in those derived from cells over-producing SLX4, might not be high enough to sufficiently compete out EXO1. *In vivo*, dampening of MMR by SLX4 must be tightly regulated and may rely on actively driven high concentrations of SLX4 at specific genomic locations or in the vicinity of replication forks that will locally impact MutSα-dependent repair. Furthermore, our data suggest that SLX4–MSH2 complex formation preferentially occurs on chromatin (Figure 1C) and there are precedents for chromatin-dependent regulation of MMR (62,63,69,70), such as the targeting of MutSα to the epigenetic mark H3K36me3 (69,70). Hence, recapitulating SLX4-driven MMR inhibition in cell-free extracts might prove particularly challenging. Alternatively, SLX4 may dampen MMR preferentially in the context of mismatches that contain a modified base such as meG-T induced by 6-TG or MNNG. However, SLX4 has been detected in an unbiased proteomic study that searched for proteins that preferentially associate with a plasmid containing an A/C mismatch in Xenopus nucleoplasmic extracts (62), suggesting that recruitment of SLX4 by MutSα and modulation of MMR is not limited to mismatches containing a modified base.

Given the primordial role of MMR repair in maintaining genome stability, it may appear surprising at first glance that evolution has selected SLX4-driven MMR inhibition. However, this is not unprecedented and other mechanisms of MMR inhibition have been described. As mentioned above, p21 inhibits PCNA function in MMR (68). Furthermore, the deacetylase HDAC6 also negatively regulates MMR by promoting MSH2 degradation (71) and preventing MLH1 binding to MutSα (72) while CAF1-mediated replication coupled chromatin assembly was proposed to limit the extent of MMR driven degradation of the nascent strand (73,74). Sequestration of MLH1 by FAN1 has recently been reported to reduce MutSβ-dependent MMR activity and prevent the expansion of CAG repeats (75). Inhibition of MMR has also been reported in pathological situations. For example, nuclear EGFR that is associated with poor outcome in various cancers (76), phosphorylates PCNA on tyrosine 211 and inhibits MMR, presumably by weakening the interaction of phosphorylated PCNA with MutSα and MutSβ (77). Overexpression of HORMAD1, a meiosis-specific protein aberrantly expressed in various cancers, was also shown to inhibit MMR through the cytosolic sequestration of the MCM9 helicase (78) that normally stimulates the chromatin recruitment of MLH1 and contributes to MMR *in vivo* (64,78). Future research will help determine in which circumstances inhibiting this crucial genome maintenance pathway is beneficial. MMR dampening by SLX4 might prove particularly relevant during meiotic recombination between homologs. In vegetative cells, MMR dampening by SLX4 may represent an important tolerance mechanism that tempers the MMR-mediated toxicity of O6-methylguanines DNA lesions that have escaped repair by the O6-methylguanine DNA methyltransferase (MGMT).

Besides characterizing a new functional interaction between SLX4 and MutSα-dependent MMR, we have generated and established the KO30 cell line as a novel mutant cellular model that expresses an N-terminally truncated variant of SLX4 (SLX4ΔNter) that starts at Met360. The recovery of such cells from experiments initially aimed at knocking-out *SLX4*, suggests that SLX4 functions critical for the viability of HeLa cells are harboured by parts of SLX4 that are downstream of the N-terminal truncation. If so, generating a *bona fide* SLX4 fully knocked-out HeLa cell line might prove challenging, if not impossible, without the recovery of hypomorphic SLX4 mutant clones that display profound ICL hypersensitivity while producing shorter C-terminal SLX4 variants (Figure 2 and Supplementary Figure S2). In line with this, it was previously reported that knocking-out SLX4 in the chicken tumoral DT40 cell line is lethal and that this does not involve the loss of SLX4 ICL repair functions (9), raising the possibility that SLX4 may also be essential in human cancer cell lines (1). The KO30 cell line represents a valuable model to better characterize the functions of the SLX4$^{1\text{-}359aa}$ N-terminal region, including those involved in ICL repair. We believe that the acute ICL hypersensitivity of KO30 cells is primarily due to the loss of the UBZ4 motifs and not to impaired SLX4–MSH2 complex formation, as it is corrected by SLX4$^{\Delta MSH2bd}$ just as well as by WT SLX4 (Figure 3). The lack of contribution of SLX4–MSH2 to cellular resistance to crosslinking agents may come as a surprise considering that both SLX4 and MSH2 contribute

to ICL repair and the known interplay between FA proteins and MMR proteins in ICL repair (40,79). However, MSH2 has been found to promote monoubiquitination of FANCD2 (39,40) whereas current evidence points rather to a role of SLX4 downstream of FANCD2 monoubiquitination (6,7,9). Interestingly, while some MMR factors contribute to ICL repair, several FA proteins have been suggested to positively contribute to MMR (40,80). Therefore, our findings that SLX4 (FANCP) instead negatively controls MMR shed new light on the functional ties between FA and MMR and suggest that investigating the multiple connections between FA and MMR proteins is a worthwhile line of research that can unravel unexpected findings.

In conclusion, our study unravels an unexpected function of SLX4 that involves MMR dampening driven by SLX4-MutSα complex formation. It provides a detailed mapping and functional analysis of the SLX4–MSH2 interaction yielding important structural insight with the identification of a conserved SHIP box within the SLX4 N-terminus. By showing that SLX4–MSH2 complex formation relies on the association of the SLX4 SHIP box with the lever 1 domain of MSH2 and that it follows the same principles than EXO1-MSH2 complex formation, our findings suggest that SLX4 negatively interferes with MMR by competing with other SHIP box containing MMR activators. Future research will be needed to better understand in which context inhibition of MMR by SLX4 is important for the maintenance of genome stability and to assess the functional ties that we suspect must exist between this mechanism and cancer biology.

DATA AVAILABILITY

The mass spectrometry data have been deposited to the ProteomeXchange Consortium via the PRIDE partner repository with the dataset identifiers PXD029062 and PXD029084.

SUPPLEMENTARY DATA

Supplementary Data are available at NAR Online.

ACKNOWLEDGEMENTS

We are grateful to Mauro Modesti, Christophe Lachaud and Vincent Pagès for sharing reagents. We thank our colleagues of the Gaillard team and the CRCM 3R community for stimulating discussions and express our gratitude to Emmanuelle Despras and Bertrand Llorente for their critical reading of the manuscript.

FUNDING

Institut National du Cancer [INCa-PLBio 2016-159; INCa-PLBio 2019-152]; Siric-Cancéropôle PACA (AAP Projets émergents 2015); Fondation pour la Recherche Médicale [AAP Equipe FRM 2020 EQU202003010245 to P.H.G.]. Funding for open access charge: AAP Equipe FRM 2020 [EQU202003010245].
Conflict of interest statement. None declared.

REFERENCES

1. Guervilly,J.-H. and Gaillard,P.H. (2018) SLX4: multitasking to maintain genome stability. *Crit. Rev. Biochem. Mol.*, **53**, 475–514.
2. Fekairi,S., Scaglione,S., Chahwan,C., Taylor,E.R., Tissier,A., Coulon,S., Dong,M.-Q., Ruse,C., Yates,J.R., Russell,P. *et al.* (2009) Human SLX4 is a holliday junction resolvase subunit that binds multiple DNA repair/recombination endonucleases. *Cell*, **138**, 78–89.
3. Svendsen,J.M., Smogorzewska,A., Sowa,M.E., O'Connell,B.C., Gygi,S.P., Elledge,S.J. and Harper,J.W. (2009) Mammalian BTBD12/SLX4 assembles a holliday junction resolvase and is required for DNA repair. *Cell*, **138**, 63–77.
4. Munoz,I.M., Hain,K., Déclais,A.-C., Gardiner,M., Toh,G.W., Sanchez-Pulido,L., Heuckmann,J.M., Toth,R., Macartney,T., Eppink,B. *et al.* (2009) Coordination of structure-specific nucleases by human SLX4/BTBD12 is required for DNA repair. *Mol. Cell*, **35**, 116–127.
5. Andersen,S.L., Bergstralh,D.T., Kohl,K.P., LaRocque,J.R., Moore,C.B. and Sekelsky,J. (2009) Drosophila MUS312 and the vertebrate ortholog BTBD12 interact with DNA structure-specific endonucleases in DNA repair and recombination. *Mol. Cell*, **35**, 128–135.
6. Hodskinson,M.R.G., Silhan,J., Crossan,G.P., Garaycoechea,J.I., Mukherjee,S., Johnson,C.M., Schärer,O.D. and Patel,K.J. (2014) Mouse SLX4 is a tumor suppressor that stimulates the activity of the nuclease XPF-ERCC1 in DNA crosslink repair. *Mol. Cell*, **54**, 472–484.
7. Klein Douwel,D., Boonen,R.A.C.M., Long,D.T., Szypowska,A.A., Räschle,M., Walter,J.C. and Knipscheer,P. (2014) XPF-ERCC1 acts in unhooking DNA interstrand crosslinks in cooperation with FANCD2 and FANCP/SLX4. *Mol. Cell*, **54**, 460–471.
8. Kim,Y., Lach,F.P., Desetty,R., Hanenberg,H., Auerbach,A.D. and Smogorzewska,A. (2011) Mutations of the SLX4 gene in fanconi anemia. *Nat. Genet.*, **43**, 142–146.
9. Yamamoto,K.N., Kobayashi,S., Tsuda,M., Kurumizaka,H., Takata,M., Kono,K., Jiricny,J., Takeda,S. and Hirota,K. (2011) Involvement of SLX4 in interstrand cross-link repair is regulated by the fanconi anemia pathway. *Proc. Natl. Acad. Sci. U.S.A.*, **108**, 6492–6496.
10. Lachaud,C., Castor,D., Hain,K., Muñoz,I., Wilson,J., MacArtney,T.J., Schindler,D. and Rouse,J. (2014) Distinct functional roles for the two SLX4 ubiquitin-binding UBZ domains mutated in fanconi anemia. *J. Cell Sci.*, **127**, 2811–2817.
11. Wang,R., Wang,S., Dhar,A., Peralta,C. and Pavletich,N.P. (2020) DNA clamp function of the monoubiquitinated fanconi anaemia ID complex. *Nature*, **580**, 278–282.
12. Katsuki,Y., Abe,M., Park,S.Y., Wu,W., Yabe,H., Yabe,M., van Attikum,H., Nakada,S., Ohta,T., Seidman,M.M. *et al.* (2021) RNF168 E3 ligase participates in ubiquitin signaling and recruitment of SLX4 during DNA crosslink repair. *Cell Rep.*, **37**, 109879.
13. Stoepker,C., Hain,K., Schuster,B., Hilhorst-Hofstee,Y., Rooimans,M.A., Steltenpool,J., Oostra,A.B., Eirich,K., Korthof,E.T., Nieuwint,A.W.M. *et al.* (2011) SLX4, a coordinator of structure-specific endonucleases, is mutated in a new fanconi anemia subtype. *Nat. Genet.*, **43**, 138–141.
14. Garner,E., Kim,Y., Lach,F.P., Kottemann,M.C. and Smogorzewska,A. (2013) Human GEN1 and the SLX4-Associated nucleases MUS81 and SLX1 are essential for the resolution of replication-induced holliday junctions. *Cell Rep.*, **5**, 207–215.
15. Wyatt,H.D.M., Sarbajna,S., Matos,J. and West,S.C. (2013) Coordinated actions of SLX1–SLX4 and MUS81-EME1 for holliday junction resolution in human cells. *Mol. Cell*, **52**, 234–247.
16. Castor,D., Nair,N., Déclais,A.-C., Lachaud,C., Toth,R., Macartney,T.J., Lilley,D.M.J., Arthur,J.S.C. and Rouse,J. (2013) Cooperative control of holliday junction resolution and DNA repair by the SLX1 and MUS81-EME1 nucleases. *Mol. Cell*, **52**, 221–233.
17. Wilson,J.S.J., Tejera,A.M., Castor,D., Toth,R., Blasco,M.A. and Rouse,J. (2013) Localization-dependent and -independent roles of SLX4 in regulating telomeres. *Cell Rep.*, **4**, 853–860.
18. Wan,B., Yin,J., Horvath,K., Sarkar,J., Chen,Y., Wu,J., Wan,K., Lu,J., Gu,P., Yu,E.Y. *et al.* (2013) SLX4 assembles a telomere maintenance toolkit by bridging multiple endonucleases with telomeres. *Cell Rep.*, **4**, 861–869.
19. Panier,S., Maric,M., Hewitt,G., Mason-Osann,E., Gali,H., Dai,A., Labadorf,A., Guervilly,J.-H., Ruis,P., Segura-Bayona,S. *et al.* (2019)

SLX4IP antagonizes promiscuous BLM activity during ALT maintenance. *Mol. Cell*, **76**, 27–43.
20. Robinson,N.J., Miyagi,M., Scarborough,J.A., Scott,J.G., Taylor,D.J. and Schiemann,W.P. (2021) SLX4IP promotes RAP1 SUMOylation by PIAS1 to coordinate telomere maintenance through NF-κB and notch signaling. *Sci. Signal*, **14**, eabe9613.
21. Robinson,N.J., Morrison-Smith,C.D., Gooding,A.J., Schiemann,B.J., Jackson,M.W., Taylor,D.J. and Schiemann,W.P. (2020) SLX4IP and telomere dynamics dictate breast cancer metastasis and therapeutic responsiveness. *Life Sci. Alliance*, **3**, e201900427.
22. Ouyang,J., Garner,E., Hallet,A., Nguyen,H.D., Rickman,K.A., Gill,G., Smogorzewska,A. and Zou,L. (2015) Noncovalent interactions with SUMO and ubiquitin orchestrate distinct functions of the SLX4 complex in genome maintenance. *Mol. Cell*, **57**, 108–122.
23. Guervilly,J.-H., Takedachi,A., Naim,V., Scaglione,S., Chawhan,C., Lovera,Y., Despras,E., Kuraoka,I., Kannouche,P., Rosselli,F. *et al.* (2015) The SLX4 complex is a SUMO E3 ligase that impacts on replication stress outcome and genome stability. *Mol. Cell*, **57**, 123–137.
24. González-Prieto,R., Cuijpers,S.A., Luijsterburg,M.S., Attikum,H. and Vertegaal,A.C. (2015) SUMOylation and PARylation cooperate to recruit and stabilize SLX4 at DNA damage sites. *EMBO Rep.*, **16**, 512–519.
25. Takedachi,A., Despras,E., Scaglione,S., Guérois,R., Guervilly,J.H., Blin,M., Audebert,S., Camoin,L., Hasanova,Z., Schertzer,M. *et al.* (2020) SLX4 interacts with RTEL1 to prevent transcription-mediated DNA replication perturbations. *Nat. Struct. Mol. Biol.*, **27**, 438–449.
26. Young,S.J., Sebald,M., Punatar,R.S., Larin,M., Masino,L., Rodrigo-Brenni,M.C., Liang,C.-C. and West,S.C. (2020) MutSβ stimulates holliday junction resolution by the SMX complex. *Cell Rep.*, **33**, 108289.
27. Peltomäki,P. (2005) Lynch syndrome genes. *Fam. Cancer*, **4**, 227–232.
28. Jiricny,J. (2006) The multifaceted mismatch-repair system. *Nat. Rev. Mol. Cell Bio.*, **7**, 335–346.
29. Kadyrov,F.A., Dzantiev,L., Constantin,N. and Modrich,P. (2006) Endonucleolytic function of mutlα in human mismatch repair. *Cell*, **126**, 297–308.
30. Modrich,P. (2006) Mechanisms in eukaryotic mismatch repair. *J. Biol. Chem.*, **281**, 30305–30309.
31. Li,G.-M. (2008) Mechanisms and functions of DNA mismatch repair. *Cell Res.*, **18**, 85–98.
32. Karran,P., Offman,J. and Bignami,M. (2003) Human mismatch repair, drug-induced DNA damage, and secondary cancer. *Biochimie*, **85**, 1149–1160.
33. Ghosal,G., Leung,J.W.-C., Nair,B.C., Fong,K.-W. and Chen,J. (2012) Proliferating cell nuclear antigen (PCNA)-binding protein C1orf124 is a regulator of translesion synthesis. *J. Biol. Chem.*, **287**, 34225–34233.
34. Zhang,H., Chen,Z., Ye,Y., Ye,Z., Cao,D., Xiong,Y., Srivastava,M., Feng,X., Tang,M., Wang,C. *et al.* (2019) SLX4IP acts with SLX4 and XPF-ERCC1 to promote interstrand crosslink repair. *Nucleic Acids Res.*, **47**, 10181–10201.
35. Burdova,K., Mihaljevic,B., Sturzenegger,A., Chappidi,N. and Janscak,P. (2015) The mismatch-binding factor mutsβ can mediate ATR activation in response to DNA double-strand breaks. *Mol. Cell*, **59**, 603–614.
36. Geng,H., Du,C., Chen,S., Salerno,V., Manfredi,C. and Hsieh,P. (2011) In vitro studies of DNA mismatch repair proteins. *Anal. Biochem.*, **413**, 179–184.
37. Laureti,L., Demol,J., Fuchs,R.P. and Pagès,V. (2015) Bacterial proliferation: keep dividing and don't mind the gap. *PLos Genet.*, **11**, e1005757.
38. Koehl,P., Burnouf,D. and Fuchs,R.P.P. (1989) Construction of plasmids containing a unique acetylaminofluorene adduct located within a mutation hot spot a new probe for frameshift mutagenesis. *J. Mol. Biol.*, **207**, 355–364.
39. Huang,M., Kennedy,R., Ali,A.M., Moreau,L.A., Meetei,A.R., D'Andrea,A.D. and Chen,C.C. (2011) Human MutS and FANCM complexes function as redundant DNA damage sensors in the fanconi anemia pathway. *DNA Repair*, **10**, 1203–1212.
40. Williams,S.A., Wilson,J.B., Clark,A.P., Mitson-Salazar,A., Tomashevski,A., Ananth,S., Glazer,P.M., Semmes,O.J., Bale,A.E., Jones,N.J. *et al.* (2011) Functional and physical interaction between the mismatch repair and FA-BRCA pathways. *Hum. Mol. Genet.*, **20**, 4395–4410.
41. Wu,Q., Christensen,L.A., Legerski,R.J. and Vasquez,K.M. (2005) Mismatch repair participates in error-free processing of DNA interstrand crosslinks in human cells. *EMBO Rep.*, **6**, 551–557.
42. Dronkert,M.L.G. and Kanaar,R. (2001) Repair of DNA interstrand cross-links. *Mutat. Res. DNA Repair.*, **486**, 217–247.
43. Karran,P. and Attard,N. (2008) Thiopurines in current medical practice: molecular mechanisms and contributions to therapy-related cancer. *Nat. Rev. Cancer*, **8**, 24–36.
44. Stojic,L., Mojas,N., Cejka,P., Pietro,M., Ferrari,S., Marra,G. and Jiricny,J. (2004) Mismatch repair-dependent G2 checkpoint induced by low doses of SN1 type methylating agents requires the ATR kinase. *Gene Dev.*, **18**, 1331–1344.
45. Mojas,N., Lopes,M. and Jiricny,J. (2007) Mismatch repair-dependent processing of methylation damage gives rise to persistent single-stranded gaps in newly replicated DNA. *Gene Dev.*, **21**, 3342–3355.
46. Goellner,E.M., Putnam,C.D., Graham,W.J., Rahal,C.M., Li,B.-Z. and Kolodner,R.D. (2018) Identification of exo1-msh2 interaction motifs in DNA mismatch repair and new Msh2-binding partners. *Nat. Struct. Mol. Biol.*, **25**, 650–659.
47. Warren,J.J., Pohlhaus,T.J., Changela,A., Iyer,R.R., Modrich,P.L. and Beese,L.S. (2007) Structure of the human mutsα DNA lesion recognition complex. *Mol. Cell*, **26**, 579–592.
48. Glaab,W.E., Risinger,J.I., Umar,A., Barrett,J.C., Kunkel,T.A. and Tindall,K.R. (1998) Resistance to 6-thioguanine in mismatch repair-deficient human cancer cell lines correlates with an increase in induced mutations at the HPRT locus. *Carcinogenesis*, **19**, 1931–1937.
49. de Wind,N., Dekker,M., Claij,N., Jansen,L., van Klink,Y., Radman,M., Riggins,G., van der Valk,M., van't Wout,K. and te Riele,H. (1999) HNPCC-like cancer predisposition in mice through simultaneous loss of msh3 and msh6 mismatch-repair protein functions. *Nat. Genet.*, **23**, 359–362.
50. Abuin,A., Zhang,H. and Bradley,A. (2000) Genetic analysis of mouse embryonic stem cells bearing msh3 and msh2 single and compound mutations. *Mol. Cell. Biol.*, **20**, 149–157.
51. Umar,A., Koi,M., Risinger,J.I., Glaab,W.E., Tindall,K.R., Kolodner,R.D., Boland,C.R., Barrett,J.C. and Kunkel,T.A. (1997) Correction of hypermutability, N-methyl-N'-nitro-N-nitrosoguanidine resistance, and defective DNA mismatch repair by introducing chromosome 2 into human tumor cells with mutations in MSH2 and MSH6. *Cancer Res.*, **57**, 3949–3955.
52. Karran,P. (2001) Mechanisms of tolerance to DNA damaging therapeutic drugs. *Carcinogenesis*, **22**, 1931–1937.
53. Yoshioka,K., Yoshioka,Y. and Hsieh,P. (2006) ATR kinase activation mediated by mutsα and mutlα in response to cytotoxic O6-methylguanine adducts. *Mol. Cell*, **22**, 501–510.
54. Yang,G., Scherer,S.J., Shell,S.S., Yang,K., Kim,M., Lipkin,M., Kucherlapati,R., Kolodner,R.D. and Edelmann,W. (2004) Dominant effects of an msh6 missense mutation on DNA repair and cancer susceptibility. *Cancer Cell*, **6**, 139–150.
55. Lin,D.P., Wang,Y., Scherer,S.J., Clark,A.B., Yang,K., Avdievich,E., Jin,B., Werling,U., Parris,T., Kurihara,N. *et al.* (2004) An msh2 point mutation uncouples DNA mismatch repair and apoptosis. *Cancer Res.*, **64**, 517–522.
56. Olivieri,M., Cho,T., Álvarez-Quilón,A., Li,K., Schellenberg,M.J., Zimmermann,M., Hustedt,N., Rossi,S.E., Adam,S., Melo,H. *et al.* (2020) A genetic map of the response to DNA damage in human cells. *Cell*, **182**, 481–496.
57. Issaeva,N., Thomas,H.D., Djureinovic,T., Djurenovic,T., Jaspers,J.E., Stoimenov,I., Kyle,S., Pedley,N., Gottipati,P., Zur,R. *et al.* (2010) 6-Thioguanine Selectively kills BRCA2-Defective tumors and overcomes PARP inhibitor resistance. *Cancer Res.*, **70**, 6268–6276.
58. Rajesh,P., Litvinchuk,A.V., Pittman,D.L. and Wyatt,M.D. (2011) The homologous recombination protein RAD51D mediates the processing of 6-Thioguanine lesions downstream of mismatch repair. *Mol. Cancer Res.*, **9**, 206–214.
59. Rajesh,P., Rajesh,C., Wyatt,M.D. and Pittman,D.L. (2010) RAD51D protects against MLH1-dependent cytotoxic responses to O6-methylguanine. *DNA Repair*, **9**, 458–467.
60. Roos,W.P., Nikolova,T., Quiros,S., Naumann,S.C., Kiedron,O., Zdzienicka,M.Z. and Kaina,B. (2009) Brca2/Xrcc2 dependent HR, but not NHEJ, is required for protection against O6-methylguanine

triggered apoptosis, DSBs and chromosomal aberrations by a process leading to SCEs. *DNA Repair*, **8**, 72–86.
61. Chen,Z., Tran,M., Tang,M., Wang,W., Gong,Z. and Chen,J. (2016) Proteomic analysis reveals a novel mutator s (MutS) partner involved in mismatch repair pathway. *Mol. Cell. Proteomics*, **15**, 1299–1308.
62. Terui,R., Nagao,K., Kawasoe,Y., Taki,K., Higashi,T.L., Tanaka,S., Nakagawa,T., Obuse,C., Masukata,H. and Takahashi,T.S. (2018) Nucleosomes around a mismatched base pair are excluded via an Msh2-dependent reaction with the aid of SNF2 family ATPase smarcad1. *Gene Dev.*, **32**, 806–821.
63. Takeishi,Y., Fujikane,R., Rikitake,M., Obayashi,Y., Sekiguchi,M. and Hidaka,M. (2020) SMARCAD1-mediated recruitment of the DNA mismatch repair protein mutlα to mutsα on damaged chromatin induces apoptosis in human cells. *J. Biol. Chem.*, **295**, 1056–1065.
64. Traver,S., Coulombe,P., Peiffer,I., Hutchins,J.R.A., Kitzmann,M., Latreille,D. and Méchali,M. (2015) MCM9 is required for mammalian DNA mismatch repair. *Mol. Cell*, **59**, 831–839.
65. Schaetzlein,S., Kodandaramireddy,N.R., Ju,Z., Lechel,A., Stepczynska,A., Lilli,D.R., Clark,A.B., Rudolph,C., Kuhnel,F., Wei,K. *et al.* (2007) Exonuclease-1 deletion impairs DNA damage signaling and prolongs lifespan of telomere-dysfunctional mice. *Cell*, **130**, 863–877.
66. Schaetzlein,S., Chahwan,R., Avdievich,E., Roa,S., Wei,K., Eoff,R.L., Sellers,R.S., Clark,A.B., Kunkel,T.A., Scharff,M.D. *et al.* (2013) Mammalian exo1 encodes both structural and catalytic functions that play distinct roles in essential biological processes. *Proc. Natl. Acad. Sci. U.S.A.*, **110**, E2470–E2479.
67. Izumchenko,E., Saydi,J. and Brown,K.D. (2012) Exonuclease 1 (Exo1) is required for activating response to SN1 DNA methylating agents. *DNA Repair*, **11**, 951–964.
68. Umar,A., Buermeyer,A.B., Simon,J.A., Thomas,D.C., Clark,A.B., Liskay,R.M. and Kunkel,T.A. (1996) Requirement for PCNA in DNA mismatch repair at a step preceding DNA resynthesis. *Cell*, **87**, 65–73.
69. Huang,Y., Gu,L. and Li,G.-M. (2018) H3K36me3-mediated mismatch repair preferentially protects actively transcribed genes from mutation. *J. Biol. Chem.*, **293**, 7811–7823.
70. Li,F., Mao,G., Tong,D., Huang,J., Gu,L., Yang,W. and Li,G.-M. (2013) The histone mark H3K36me3 regulates human DNA mismatch repair through its interaction with MutSα. *Cell*, **153**, 590–600.
71. Zhang,M., Xiang,S., Joo,H.-Y., Wang,L., Williams,K.A., Liu,W., Hu,C., Tong,D., Haakenson,J., Wang,C. *et al.* (2014) HDAC6 deacetylates and ubiquitinates MSH2 to maintain proper levels of MutSα. *Mol. Cell*, **55**, 31–46.
72. Zhang,M., Hu,C., Moses,N., Haakenson,J., Xiang,S., Quan,D., Fang,B., Yang,Z., Bai,W., Bepler,G. *et al.* (2019) HDAC6 regulates DNA damage response via deacetylating MLH1. *J. Biol. Chem.*, **294**, 5813–5826.
73. Kadyrova,L.Y., Dahal,B.K. and Kadyrov,F.A. (2016) The major replicative histone chaperone CAF-1 suppresses the activity of the DNA mismatch repair system in the cytotoxic response to a DNA-methylating agent. *J. Biol. Chem.*, **291**, 27298–27312.
74. Kadyrova,L.Y., Blanko,E.R. and Kadyrov,F.A. (2011) CAF-I-dependent control of degradation of the discontinuous strands during mismatch repair. *Proc. Natl. Acad. Sci. U.S.A.*, **108**, 2753–2758.
75. Goold,R., Hamilton,J., Menneteau,T., Flower,M., Bunting,E.L., Aldous,S.G., Porro,A., Vicente,J.R., Allen,N.D., Wilkinson,H. *et al.* (2021) FAN1 controls mismatch repair complex assembly via MLH1 retention to stabilize CAG repeat expansion in huntington's disease. *Cell Rep.*, **36**, 109649.
76. Brand,T.M., Iida,M., Luthar,N., Starr,M.M., Huppert,E.J. and Wheeler,D.L. (2013) Nuclear EGFR as a molecular target in cancer. *Radiother. Oncol.*, **108**, 370–377.
77. Ortega,J., Li,J.Y., Lee,S., Tong,D., Gu,L. and Li,G.-M. (2015) Phosphorylation of PCNA by EGFR inhibits mismatch repair and promotes misincorporation during DNA synthesis. *Proc. Natl. Acad. Sci. U.S.A.*, **112**, 5667–5672.
78. Liu,K., Wang,Y., Zhu,Q., Li,P., Chen,J., Tang,Z., Shen,Y., Cheng,X., Lu,L.-Y. and Liu,Y. (2020) Aberrantly expressed HORMAD1 disrupts nuclear localization of MCM8–MCM9 complex and compromises DNA mismatch repair in cancer cells. *Cell Death. Dis.*, **11**, 519.
79. Peng,M., Litman,R., Xie,J., Sharma,S., Brosh,R.M. and Cantor,S.B. (2007) The FANCJ/MutLα interaction is required for correction of the cross-link response in FA-J cells. *EMBO J.*, **26**, 3238–3249.
80. Xie,J., Guillemette,S., Peng,M., Gilbert,C., Buermeyer,A. and Cantor,S.B. (2010) An MLH1 mutation links BACH1/FANCJ to colon cancer, signaling, and insight toward directed therapy. *Cancer Prev. Res.*, **3**, 1409–1416.
81. Jehl,P., Manguy,J., Shields,D.C., Higgins,D.G. and Davey,N.E. (2016) ProViz—a web-based visualization tool to investigate the functional and evolutionary features of protein sequences. *Nucleic Acids Res.*, **44**, W11–W15.
82. Crooks,G.E., Hon,G., Chandonia,J.-M. and Brenner,S.E. (2004) WebLogo: a sequence logo generator. *Genome Res.*, **14**, 1188–1190.